CHAPTER 5

Quantitative Assessment of Spinal Cord Injury

Hasan Al-Nashash[1], Hasan Mir[1], Anil Maybahate[2], Nitish Thakor[2], Angelo All[2]

[1]*Department of Electrical Engineering, American University of Sharjah, Sharjah, UAE*
[2]*Department of Biomedical Engineering, Johns Hopkins University, School of Medicine, 720 Rutland Ave. Traylor #710-B, Baltimore, MD 21205*

CONTENTS

1. INTRODUCTION

The spinal cord is a tubular bundle of millions of nerve fibers about the diameter of a human finger, surrounded by a clear fluid called cerebral spinal fluid (CSF) and protected by the bony vertebral column [1]. The length of the spinal cord is around 45 cm in men and 43 cm in women, making it shorter than the bony spinal column. The brain and spinal cord make up the central nervous system, which supports the cells extending from the brain cells down to the space between the first and second lumbar vertebrae terminating in the fibrous filum terminale. There are 31 different segments in the human spinal cord, where each left and right segment has sensory and motor nerves as shown in Figure 1 [2]. There are 8 cervical (C), 12 thoracic (T), 5 lumbar (L), 5 sacral (S), and 1 pair of coccygeal nerves [1].

ISBN: x-xxxxx-xxx-x

Distributed Diagnosis and Home Healthcare
Edited by E. Y. K. Ng, U. Rajendra Acharya, and Toshiyo Tamura
Volume 3: Pages 1–17

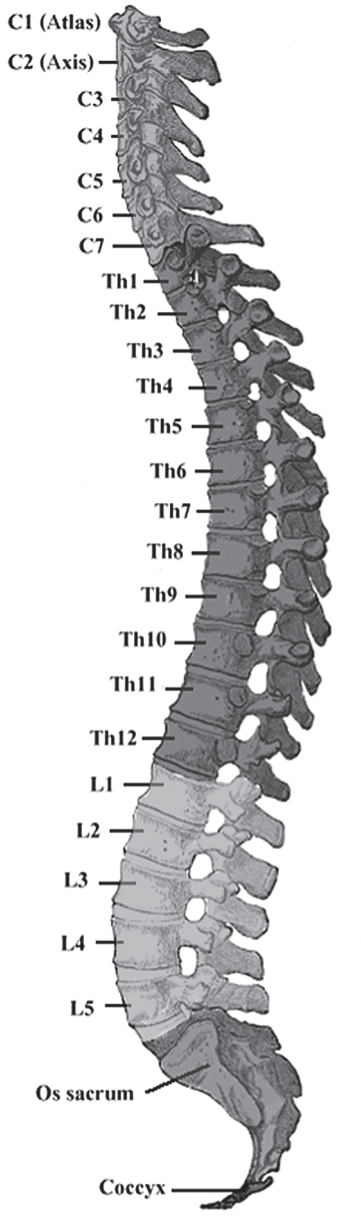

Figure 1. General scheme of the human spinal cord [2].

The spinal cord serves as the transmission pathway for all electrical activities including motor and sensory information between the central and peripheral nervous systems [3]. In addition, it serves as a center for coordinating certain reflexes. Any partial or complete injury to the spinal cord will impair the transmission, leading to the loss of sensory and/or motor functions. According to the U.S. National Spinal Cord Injury Statistical Center in Alabama, it is estimated that the annual incidence of spinal cord injury (SCI) not counting those who die is approximately 12,000 new cases each year [4]. In China, it is estimated that there are approximately 60,000 SCI incidents every year [5]. Hence there are millions of patients in the world living with the devastating effects of spinal cord injury.

What is required is an objective quantitative assessment method that enables researchers in the area of SCI recovery and rehabilitation to accurately and objectively assess the level of SCI and evaluate the effectiveness of any possible therapeutic mechanisms. It is important to know that a small number of spared spinal cord fibers with immediate treatment can greatly improve the quality of life of patients with SCI.

Researchers use alternative electrophysiological [6–8] and imaging [9, 10] techniques for the assessment of SCI. The standard assessment imaging modalities include X-rays, computed tomography (CT) scan, and magnetic resonance imaging (MRI). While X-ray imaging is used to determine the site of fracture, CT and MRI studies are used to assess the level of injury of spinal cord soft tissues. MRI provides anatomical information which enables physicians to precisely locate the site of the injury. It does not, however, provide quantitative information on the functional integrity of the spinal cord [9, 10].

There are other techniques that are more applicable to animal SCI models such as the conventional subjective Basso, Beattie, and Bresnahan (BBB) method [11, 12]. A neurologist would observe the animal behavior in an open field for four minutes and give a score ranging from 0 to 21. The BBB score is an observational measure that reflects the animal's locomotor capabilities. Clearly a complementary objective quantitative assessment method of SCI is required.

One powerful technique used in both human and animal SCI studies is the Evoked Potential (EP), which reflects the electrophysiological response of the neural system to an external stimulus. Somatosensory evoked potentials (SEPs) are obtained by electrical stimulation of the median nerve at the wrist or the posterior tibial nerve at the ankle. Different researchers process the SEP data for SCI detection and assessment using alternative temporal, parametric, and spectral techniques. Some SEP signals do not have a detectable latency or peak amplitude following severe spinal cord injury [13, 14].

In this chapter, several alternative methods based on SEP signals to quantify the level of spinal cord injury are presented. These methods are spectral coherence, correlation-based metric, entropy-based metric, and morphological analysis. These methods have the advantages of being objective and quantitative, and they do not require a trained examiner and do not necessarily require the pre-injury signals.

This chapter is organized into four sections. In Section 2, the protocol and data collection methods are detailed. In Section 3 quantification methods are described with results obtained from rodents that were exposed to various degrees of SCI. Finally, discussion and conclusions are detailed in Section 4.

2. PROTOCOL AND DATA COLLECTION

2.1. Vertebrate Animals

Adult Lewis female rats weighing $220 \pm \sim 10$ g are studied in this project [15]. Rats are used for this model for the following reasons: (1) similarity of cranial circulation in rats and humans, (2) suitability for performing behavioral, cellular, electrophysiological, and neuro-anatomical investigations in rats, (3) considerable prior knowledge of the neuroanatomy and physiology of rats, (4) ease of obtaining cortical electrical recordings in rats, and (5) familiarity of experimenters with this species.

2.1.1. General Surgical Preparation

The rat is held in a transparent chamber with 3% isofluorane gas anesthesia and room air flow, and is removed from the chamber at the onset of drowsiness. Its mouth and nose is then placed within an anesthesia mask (using a rodent size diaphragm that fits well and uses a C-Pram circuit designed to deliver and evacuate the gas through one tube), which is connected to a mixed flow of 1.5% isofluorane, 80% oxygen and room air with a flow rate of 2 L/min. The rat is also placed on a blanket which is connected to a heating pump to maintain body temperature at $37°C \pm 0.5°C$ throughout the entire experiment. An incision is then made on the skin of the rat's head, and the tissue under the skin is removed to clean the cranium bone. Four burr holes are drilled into the cranium near the forelimb and hindlimb somatosensory and motor cortex area on the right and left hemispheres. A fifth hole is made on the frontal lobe and is used as the reference electrode. These five implanted screw electrodes make very light contact with the dura mater, and will not compress the dura or brain structures. They are fixed with dental

cement and are used for EP signal monitoring. Finally, the skin wound on the head is closed and 2% Lidocaine gel is applied.

To generate stimulation for SEP, four pairs of 1-cm stainless-steel stimulating needle electrodes are placed in proximity to the tibial nerve in the right and left hindlimb as well as the median nerve in the right and left forelimb. The needle electrodes are connected to a stimulus generator. The cranium screw electrodes are connected to an amplifier for recording the SEP signals. SEP measurements will be obtained by setting the four limb stimulus generators to generate stimulating pulses of 3.5 mA, pulse width 200 μs and presentation rate of 1 Hz in an alternating manner (right forelimb, left forelimb, left hindlimb, right hindlimb, etc.). The Lab Windows program will control the stimulator. The stimulator trigger will be followed by data acquisition. SEP signals will be recorded continuously via the amplifier and data acquisition setup.

To generate stimulation for MEP, two cranial screw electrodes are implanted over the hindlimb region of the sensorimotor cortex. (2–3 mm posterior to bregma, 1–2 mm lateral to midline). These serve as the anodes for stimulation. A third electrode is implanted on the frontal lobe and is used as the reference electrode. These screws are then connected to a stimulator (DS3 from Digitimer Ltd.), which is controlled by an RP2 Processor from TDT systems. Signals are recorded using a needle electrode, which is inserted into the tibialis anterior muscle of the rat hindlimb. A reference electrode is inserted into the footpad as well. A ground needle electrode is inserted in the dorsum of the neck. Signal acquisition uses the RA16 Medusa Base Station and the RA4 Pre-Amplifier (TDT systems). Stimulation and data acquisition is controlled by the OpenEx software suite. The stimulus comprises short trains of low intensity pulses, ranging from 5–12 mA, with pulse width of 100 μs and presentation rate of 15.1 Hz. Stimulus is presented at 1–2 mA above threshold intensity for each rat. Threshold intensity is defined as the stimulus intensity such that a train of 14 impulses elicits a signal greater than 5 μV.

2.1.2. Motor Behavioral Assessment Methods—BBB Scores

Prior to injury, rats will be tested for locomotor function. The Basso, Beattie and Bresnahan (BBB) test will be used to assess joint movement, hindlimb movements, stepping, limbs coordination, trunk position, paw placement, and tail position. The recovery after SCI in rats will be scaled from 0 to 21. Early Phase of recovery consists of isolated joint movements (score 0–7). Intermediate Phase represents a gradual improvement to consistent fronthind limbs coordination (score 8–13). Late Phase of recovery consists of a further development of plantar steps with paw coordination and tail balancing off the ground (scores 14–21). Statistical differences between rat groups in BBB score will be analyzed for recovery. Assessments will be performed concurrently with SEP and MEP monitoring.

2.1.3. Contusion Injury

NYU-impactor will be used to induce the contusion injury in rats. The contusion model of SCI accounts for more than 65% of total SCI in humans and is a clinically relevant model. The injury is reproducible and evolution of injury in the animal model is similar to that in humans. Laminectomy is performed between thoracic vertebra T6 and T10 to expose the dorsal surface of the spinal cord. The spinal cord at T8 is placed directly under the vertical shaft of the NYU mechanical impactor, and then the shaft (tip diameter of 1 mm) is slowly lowered until the tip touches the cord at which time a transducer arm sends a signal to the device indicating that contact has been made. Next, the impactor probe is withdrawn to the desired impact drop distance (12.5 mm for moderate or 25.0 mm for severe injury). After setting the computer to record the dynamics of the impact trajectory, a pin suspending the impact shaft is released and allowed to descend by gravity to hit the cord. The impactor is then withdrawn and the animal is removed from the device. Then, muscle layers and skin are sutured closed in layers. The contusion impact velocity and compression is monitored to guarantee consistency between animals.

2.1.4. Survival Protocol

Rats generally regain consciousness 30 minutes after EPs recording is complete. For hydration, the rats receive subcutaneous injections of isotonic saline, 20 ml/kg s.c. administered 12 hours after injury and repeated daily. Rats have free access to food and water during the observation period. After the spinal cord injury is induced in rats, their bladders are emptied manually twice a day, until spontaneous voiding returns. The care and treatment of animals is in strict accordance with the guidelines set by the NIH Guide for the Care and Use of Laboratory Animals, the Guidelines for the Use of Animals in Neuroscience Research and the Johns Hopkins University IACUC. Rats are housed according to IACUC—JHU, NIH and USDA guidelines.

2.1.5. Pain and Distress

Anesthesia will be used during all surgical and monitoring procedures to avoid any pain or distress to the animal. For survival experiments, topical analgesic (Lidocaine 2% gel) will be applied on the sites on the femoral and skull incision areas. Buprenex is given post-operatively twice a day for three days to relieve pain from para-vertebral muscle. Liquid Tylenol is given for 7 days. Gentamicin antibiotic is given post-surgery for one week. Rats are never allowed to regain consciousness throughout the experiment.

2.1.6. Method of Euthanasia

The animal will be deeply anesthetized and then euthanized via. transcardial perfusion with formaldehyde. The rats' spinal cords will then be harvested for histological studies.

3. QUANTIFICATION TECHNIQUES

3.1. Spectral Coherence Method

Spectral coherence is a quantitative measure that reflects the degree of similarity between any two signals [16]. The magnitude-squared spectral coherence $\gamma^2_{xy}(\omega)$ function of signals x and y is a normalized version of the cross power spectral density between x and y and is defined as [17]:

$$\gamma^2_{xy}(\omega) = \frac{|P_{xy}(\omega)|^2}{P_{xx}(\omega)P_{yy}(\omega)} \tag{1}$$

where $P_{xy}(\omega)$ is the cross power spectrum between x and y signals, $P_{xx}(\omega)$ is the power spectrum of x signal and $P_{yy}(\omega)$ is the power spectrum of the y signal.

In SCI studies, assume that a 1 pulse per second stimulus signal $I(n)$ is applied to any of the forelimbs or hindlimbs as shown in Figure 2. Let $x(n)$ and $y(n)$ be the SEP signals recorded at the cortex obtained from stimulating combinations of right forelimb, right hindlimb, left forelimb, and left hindlimb. These signals contain additive independent noise $v_1(n)$ and $v_2(n)$, but are related to $I(n)$ through linear systems $H_1(e^{j\omega})$ and $H_2(e^{j\omega})$ respectively.

If both $H_1(e^{j\omega})$ and $H_2(e^{j\omega})$ have no zeros on the unit circle with $H(e^{j\omega}) = H_2(e^{j\omega})/H_1(e^{j\omega})$, and the total noise spectrum $\tilde{v}(e^{j\omega}) = H_1(e^{j\omega})(\tilde{v}_2(e^{j\omega}) - \tilde{v}_1(e^{j\omega}))$, then it can be shown that the magnitude-squared spectral coherence γ^2_{xy} function is [18]:

$$\gamma^2(e^{j\omega}) = \frac{|H(e^{j\omega})P_{xx}(e^{j\omega})|^2}{P_{xx}(e^{j\omega})|H(e^{j\omega})|^2[P_{xx}(e^{j\omega}) + P_{vv}(e^{j\omega})]} \tag{2}$$

In a normal healthy spinal cord transmission system, $H(e^{j\omega})$ is finite with a fixed frequency transfer characteristic. Hence, with low noise power density resulting from ensemble averaging, it is expected that $\gamma^2(e^{j\omega})$ will approach unity. If SCI exists, $H(e^{j\omega})$ will be modified, and the signal power $P_{yy}(e^{j\omega})$ will be primarily due to the uncorrelated noise power. Consequently, $\gamma^2(e^{j\omega})$ will decrease and may reach zero under severe SCI conditions.

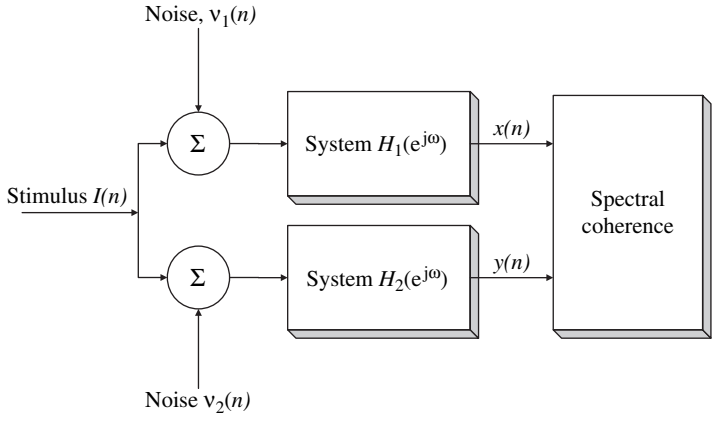

Figure 2. Model showing the stimulus signal passing through two biological systems H1 and H2.

Spectral coherence was used to study the SEP signals recorded from 15 female adult Fischer rodents before and after spinal cord injury (SCI). It is expected that the SCI injury would affect mostly the hindlimbs and not the forelimbs. Hence, the spectral coherence was calculated from SEP signals obtained from stimulating the right hindlimb and left forelimb. Figure 3 shows the spectral coherence obtained from 5 sample animals with no (control), mild (6.25 mm), moderate (12.5 mm), severe (25 mm), and very severe (50 mm) spinal cord injury. The spectral coherence variations over time before and after injury help us detect and quantify the level or severity of SCI. The spectral coherence obtained from the control animal is relatively high ($\geq$0.7) before and after laminectomy.

In the case of mild injury, the spectral coherence drops to 0.3 one week after injury but quickly recovers to a steady state above 0.6 after week 4. The spectral coherence in moderate, severe, and very severe SCI dropped to below 0.4 and did not show any signs of recovery in the weeks that followed SCI.

It is of prime importance to say that spectral coherence gave normalized, quantifiable results that did not need the baseline and did not require a trained eye.

3.2. Time-Domain Quantification Metrics

This section describes methods that attempt to quantify the similarity between two signals using only their time-domain characteristics [19, 20]. The first method, known as the adaptive signed correlation index, uses an adaptive definition of a "template" through a trichotomization procedure, and can thus be made sensitive to specific features of the reference SEP signal. The second method uses an entropy-based measure to quantify the

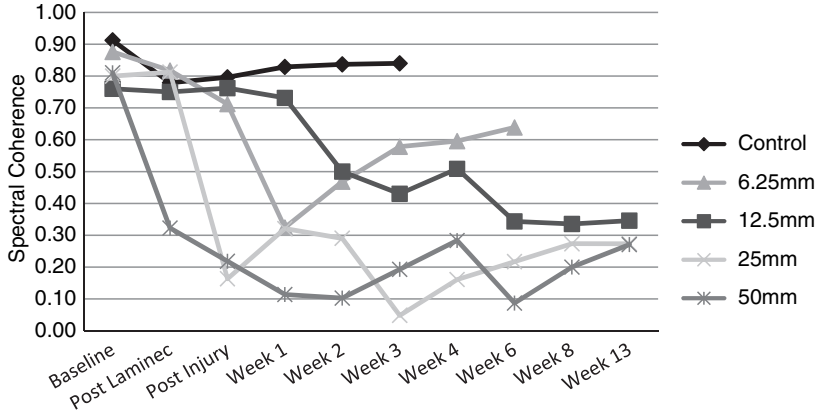

Figure 3. Spectral coherence obtained from 5 sample animals: control, mild (6.25 mm), moderate (12.5 mm), severe (25 mm), and very severe (50 mm) spinal cord injury.

level of similarity between two signals by assessing the similarity of the time-domain amplitude histogram of two signals. These two metrics are now discussed in further detail.

3.2.1. Correlation-Based Metric

Let S denote the signal space, and consider two signals $s_n^{(1)}, s_n^{(2)} \in S$. A commonly used criteria to quantify the similarity between $s_n^{(1)}$ and $s_n^{(2)}$ is the Pearson correlation coefficient (PCC), defined as

$$\rho(s_n^{(1)}, s_n^{(2)}) = \frac{\sum_n s_n^{(1)} s_n^{(2)}}{\sqrt{\sum_n s_n^{(1)} s_n^{(1)} \sum_n s_n^{(2)} s_n^{(2)}}} \tag{3}$$

An important deficiency of this metric is its lack of sensitivity to amplitude (scaling) differences. In the context of SEP signals, amplitude differences may be an indicator of the integrity of the signal pathway and hence level of SCI. Application of the PCC is thus not well suited for quantifying the similarity between SEP signals.

In order to develop a correlation metric that is sensitive to amplitude differences, consider first the set $L = \{-1, 0, +1\}$. A trichotomization mapping $S \to L$ for $s_n \in S$ and $\tilde{s}_n \in L$ is defined as

$$\tilde{s}_n = \begin{cases} +1 & s_n \in S_+ \\ 0 & s_n \in S_0 \\ -1 & s_n \in S_- \end{cases}$$

The quantities S_+, S_0, and S_- are termed the positive, zero, and negative subspace, respectively, of S. The definitions of these subspaces are not unique; in this section, they are defined through four signals $u_n^{(-)}$, $u_n^{(+)}$, $l_n^{(+)}$, $l_n^{(-)}$ such that

$$\begin{aligned} S_+ &= \{l_n^{(+)} < s_n < u_n^{(+)}\} \\ S_0 &= \{l_n^{(-)} < s_n < l_n^{(+)}\} \cup \{u_n^{(+)} < s_n < u_n^{(-)}\} \\ S_- &= \{s_n < l_n^{(-)}\} \cup \{u_n^{(-)} < s_n\} \end{aligned}$$

This subspace definition is illustrated in Figure 4.

From Figure 4, it can be seen that the subspaces are mutually exclusive and that their union results in the whole signal space S. Using the above development, the adaptive signed correlation index (ASCI) [19, 21] is defined as

$$\alpha(s_n^{(1)}, s_n^{(2)}) = \frac{\sum_n (\delta_{\tilde{s}_n^{(1)}, \tilde{s}_n^{(2)}} - \delta_{\tilde{s}_n^{(1)} \tilde{s}_n^{(2)}, -1})}{\sqrt{\sum_n (\delta_{\tilde{s}_n^{(1)}, \tilde{s}_n^{(1)}} - \delta_{\tilde{s}_n^{(1)} \tilde{s}_n^{(1)}, -1})} \sqrt{\sum_n (\delta_{\tilde{s}_n^{(2)}, \tilde{s}_n^{(2)}} - \delta_{\tilde{s}_n^{(2)} \tilde{s}_n^{(2)}, -1})}} \tag{4}$$

where $\delta_{i,j}$ is the Kronecker delta function

$$\delta_{i,j} = \begin{cases} 1 & i = j \\ 0 & i \neq j \end{cases}$$

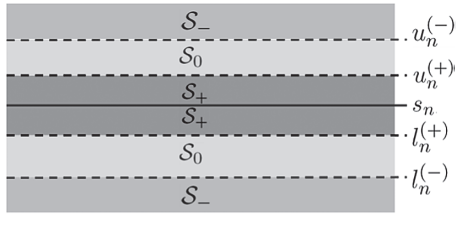

Figure 4. An illustration defining the signal subspace.

Inspection of Eq. (4) reveals that there are three effective classifications of the signal pair $s_n^{(1)}$ and $s_n^{(2)}$:

- *Concordant*, in which both elements of the pair fall in the same subspace, thus pushing α closer to $+1$
- *Nilcordant*, in which one element is in S_0, thus pushing α closer to 0
- *Discordant*, in which one element is in S_+ and one element is in S_-, thus pushing α closer to -1

The final value of α depends on the distribution of these various classifications, which in turn depend on the degree of morphological similarity of the signal pair. Thus, the ASCI has the potential to provide a more robust assessment of SCI compared to the conventional PCC.

3.2.2. Entropy-Based Metric

Consider a random message source with underlying distribution p_i. The *information* associated with the message i is defined as

$$I(i) = \log_2 \frac{1}{p_i} \tag{5}$$

where $I(i)$ is measured in bits. This definition of information fits with an intuitive notion: Messages with low probability result in high information values, whereas messages with high probability yield low information values. The *entropy* of a distribution p_i is a measure of the amount of uncertainty associated with p_i. Consequently, it is defined as the average value (expected value) of the information content of a message drawn from the source, that is

$$H(p) = E\{I(i)\} = \sum_i p_i \log_2 \frac{1}{p_i} \tag{6}$$

Entropy is often explained as the minimum number of bits required to code a message from a source with probability distribution p_i. Suppose, however, that the probability distribution is assumed to be different from p_i; that is, it is assumed to be another distribution q_i. If coding is performed on a message originating from a source with distribution p_i but assuming a distribution q_i, then the additional number of bits required to code the message is given by [22].

$$H(p, q) = \sum_i p_i \log_2 \frac{1}{q_i}$$

where $H(p, q)$ is called the *cross-entropy*. Thus, the additional number of bits required to encode a message based on this erroneous assumption of the distribution is given by

$$D(p\|q) = \sum_i p_i \log_2 \frac{p_i}{q_i} = \sum_i p_i \log_2 \frac{1}{q_i} - \sum_i p_i \log_2 \frac{1}{p_i} = H(p, q) - H(p) \tag{7}$$

where Eq. (7) is known as the *Kullback–Leibler divergence* (KLD) [20, 23] and is measured in bits. Thus, the KLD is often used to quantify the difference between two probability distributions.

Now consider again the signal pair $s_n^{(1)}$ and $s_n^{(2)}$. Suppose that signal pair $s_n^{(1)}$ represents the SEP signal measurement taken from a reference (healthy) spinal pathway, and $s_n^{(2)}$ represents the SEP signal measurement from an SCI affected pathway. Furthermore, suppose that $s_n^{(1)}$ and $s_n^{(2)}$ have amplitude histograms that follow distributions q_i and p_i, respectively. The KLD can be used to quantify the level of SCI, since SEP data obtained from baseline and non-injured spinal cords will lead to similar distributions for q_i and p_i, resulting in a low KLD value, while signals from a pathway with moderate, severe, and very severe injuries will have a distribution highly dissimilar to q_i, leading to high values of the KLD.

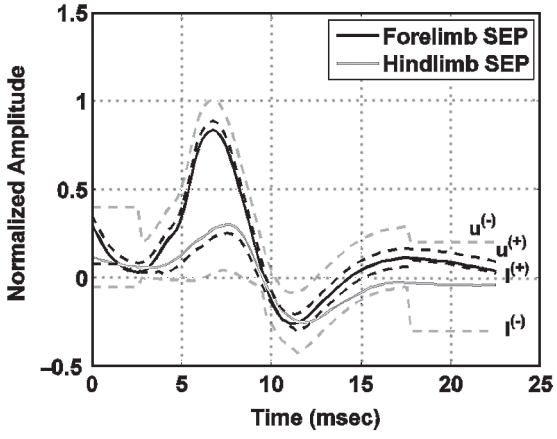

Figure 5. Typical templates and SEP signals for moderate SCI.

The data used in this section was collected as described in Section 2. SEP signals for the forelimbs and hindlimbs were collected at various stages of SCI on adult female Fischer rats. The forelimb SEP signal is considered as a reference (healthy) signal, since injury is inflicted below the forelimb (at T8-T9) and thus does not impair the forelimb spinal pathway. Because the hindlimb SEP signal must travel through the demyelinated (injured) section of the spinal pathway, however, it contains information pertinent to the severity of SCI. Thus, in this section, the value of the ASCI and KLDs will be computed for SEP signals collected on a representative rodent sample. Note that the SEP data acquired from forelimbs act as an internal control. In view of the degree of demyelination, comparison is performed for three severities of chemical injuries in SCI, termed moderate, severe, and very severe.

Typical SEP signals and subspace definitions for various stages of SCI are shown in Figures 5–7. A characteristic in the forelimb SEP signal exhibited in nearly all of the rodents tested is the presence of an upward peak followed by a downward peak. These peaks are thus selected as the critical features of a healthy SEP signal. Accordingly, the signals $u_n^{(+)}$ and $l_n^{(1)}$ were selected to emulate the shape of forelimb SEP, while allowing for some amplitude difference. The signals $u_n^{(-)}$ and $l_n^{(-)}$ were selected to be offset from $u_n^{(+)}$ and $l_n^{(+)}$, but made more permissive toward the beginning of the first peak and the end of the second peak in order to de-emphasize transient/settling effects. The selection for $u_n^{(-)}$, $u_n^{(+)}$, $l_n^{(+)}$, $l_n^{(+)}$ is constrained to be identical for all levels of SCI, as can be seen

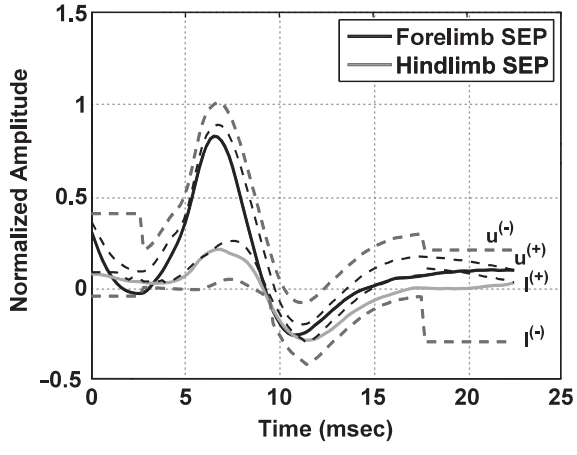

Figure 6. Typical templates and SEP signals for severe SCI.

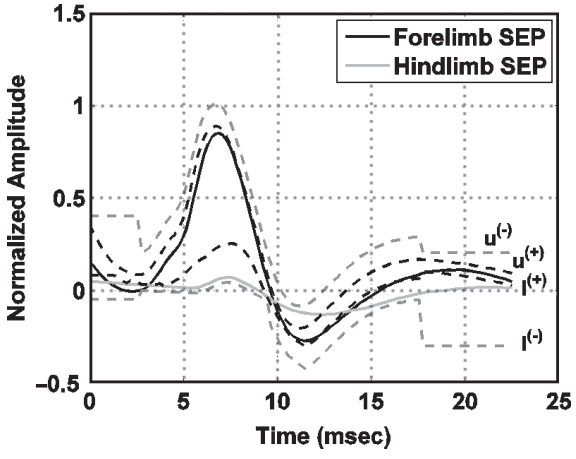

Figure 7. Typical templates and SEP signals for very severe SCI.

in Figures 5–7. This constraint, along with the high degree of similarity between the forelimb SEPs, ensures that there will be no false increase in the ASCI value.

Representative SEP signals and their amplitude histograms are shown in Figures 8–10 It can be observed from these figures, as well as from Figures 5–7, that the forelimb SEP signal is very consistent across injury levels. This indicates that the forelimb SEP signal is not affected by SCI inflicted below the forelimb, and lends further credence to its use as a reference SEP signal. As can also be seen in Figures 5–10, the strength of the evoked potential for hindlimb SEP signals decreases as the severity of injury in the spinal cord increases. This leads to a concentration of lower amplitude values, resulting in amplitude histograms increasingly dissimilar to the forelimb amplitude histograms.

Table 1 provides a comparison of the average PCC, ASCI, and KLD values using the forelimb and hindlimb SEP signals for the various degree of demyelination in SCI. It is apparent that the PCC yields very high and similar values across different degree of

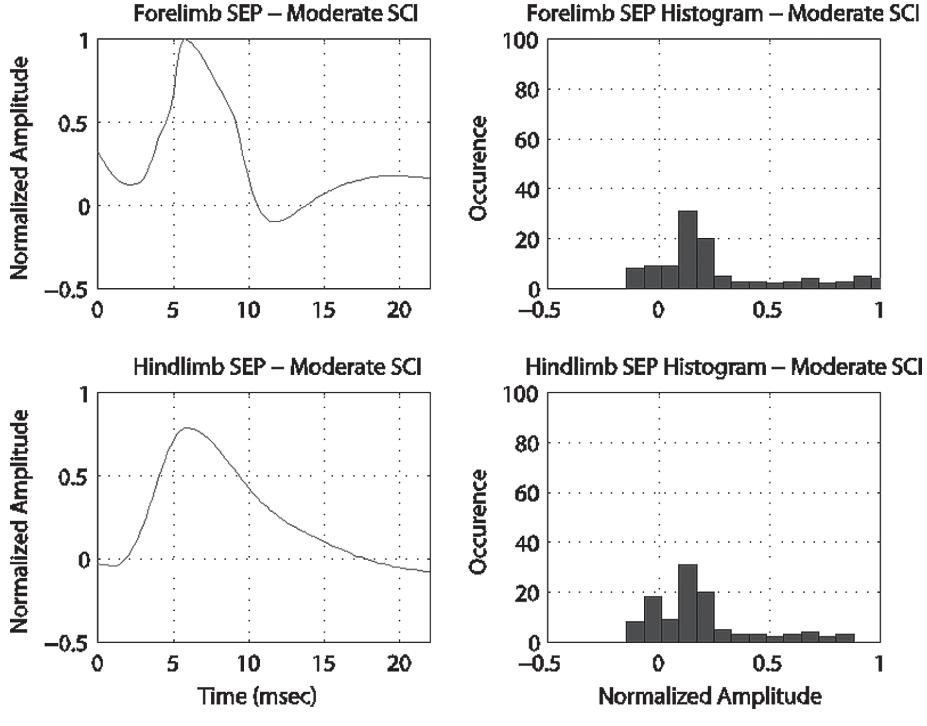

Figure 8. Typical SEP signals and amplitude histograms for moderate SC.

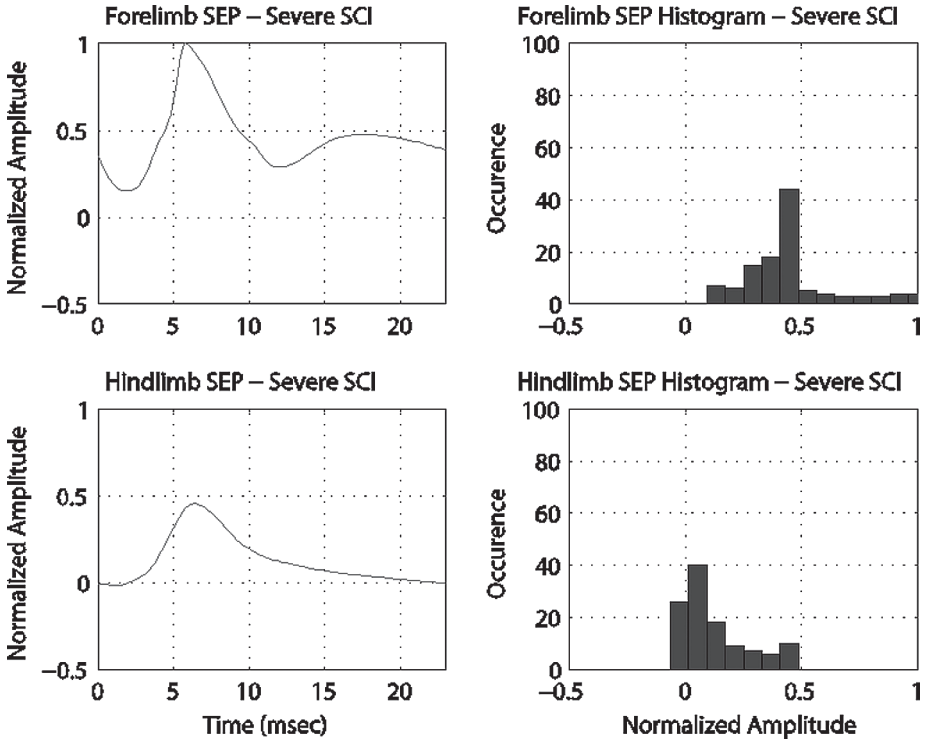

Figure 9. Typical SEP signals and amplitude histograms for severe SCI.

demyelination, an artifact of the insensitivity of the PCC to amplitude differences. In contrast, both the ASCI and KLD yield values that are more representative of the degree of morphological similarity, and this provides a clear indication of the level of SCI. This is true for both the magnitude as well as the variability of the ASCI and KLD across the

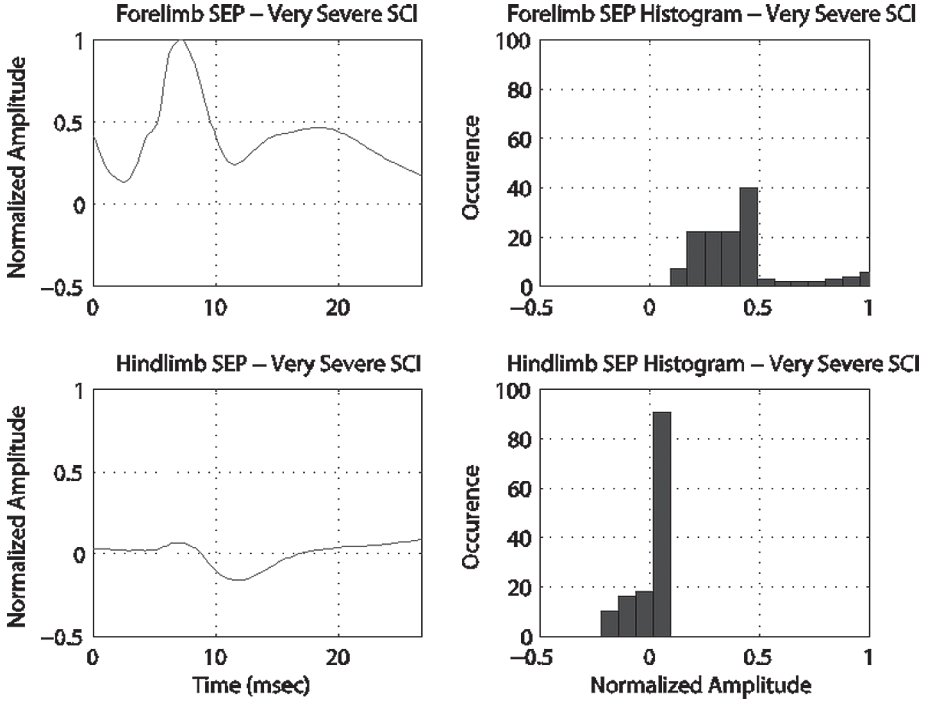

Figure 10. Typical SEP signals and amplitude histograms for very severe SCI.

Table 1. Comparison of SCI levels and metric.

Metric	Moderate SCI	Severe SCI	Very severe SCI
PCC	0.92	0.86	0.82
ASCI	0.28	0.35	0.52
KLD (bits)	0.59	2.31	6.47

extent of demyelination. This sensitivity to scaling clearly gives the ASCI and KLD an advantage over the PCC, especially in a clinical setting where amplitude differences are important.

As noted in Ref. [21], the need for defining the signal subspaces may appear to be a limitation of ASCI; however, a priori knowledge of the morphological characteristics of the "reference" signal can be taken advantage of to develop a customized subspace that is robust to signal variations. Moreover, the trichotomization procedure allows for calculation of the ASCI without any floating point operations, thus making it an attractive option for low-power, embedded medical applications.

3.3. Morphological Analysis of Somatosensory Evoked Potentials

Note that many of the techniques described above require sophisticated peak detection algorithms, and/or do not characterize the entire shape of the SEPs. The standard peak-detection-based techniques will still need human inspection making them subjective and variable. On the other hand, despite important previous studies about how the absence of some SEP peaks could prognosticate bad outcomes, there is a general absence of sensitive techniques that could confirm such an absence by going beyond traditional peak detection and assessing the entire morphology of an evoked potential response. We developed two such techniques and will briefly describe them below.

3.3.1. The Slope Analysis of SEP

In this method, we propose the use of a differential operator for transforming the signal and characterize the entire shape of the signal. Thus the slope $\delta[k]$ of a signal $x[k]$ over two consecutive samples was computed using:

$$\delta[k] = \frac{x[k+1] - x[k]}{(k+1) - k} \quad \text{for } k = 1, 2, \ldots, N \tag{8}$$

where N is the total number of samples in the signal. The corresponding angular orientation $\theta[k]$ was calculated as:

$$\theta[k] = \tan^{-1}(\delta[k]) \quad \text{for } k = 1, 2, \ldots, N \tag{9}$$

The first derivative of signals is usually very noisy as this operation amplifies high-frequency signal noise. To solve this problem, the slopes were binned along the waveform into time bins of L samples and the mean of the slopes $\delta_{\text{mean}}[j]$ was computed within each time bin as:

$$\delta_{\text{mean}}[j] = \frac{1}{L}\sum_{i=1}^{L} \delta[i + L \times (j-1)] \quad \text{for } j = 1, 2, \ldots, M \tag{10}$$

where $M = N/L$ is the total number of time bins in the signal. Besides decreasing noise, the binning and averaging procedure also has the advantage of reducing the dimensionality of the transformed signal, hence allowing easier computation in this lower dimension space.

From the mean slope $\delta_{\text{mean}}[j]$, the mean angular orientation $\theta_{\text{mean}}[j]$ was obtained using Eq. (10) above. We shall refer to $\theta_{\text{mean}}[j]_{j=1,\ldots,M}$ as the mean slope vector Θ. To measure the

similarity between any two obtained mean slope vectors Θ_i and Θ_j, the cosine distance between them was computed as [24]:

$$d(i, j) = 1 - \frac{\Theta_i^T \Theta_j}{\sqrt{\Theta_i^T \Theta_i}\sqrt{\Theta_i^T \Theta_j}} \tag{11}$$

A slope histogram shown in Figure 11 was constructed for the SEP signal by clustering the angular orientations $\theta[k]_{k=1,\ldots,N}$ into time bins of 2 msec and angle bins of 5 degrees. The mean slope vectors Θ_{pre} and Θ_{post} were constructed for the SEP signals for pre-injury and post-injury stages, respectively, using $L = 10$ corresponding to time duration of 2 msec, as shown in Figure 11.

The mean difference between the absolute mean slope vectors, $|\Theta_{\text{pre}}|$ and $|\Theta_{\text{post}}|$, across all the rats was checked for significance using a student's paired sample two-tailed t-test. The major part of the SEP signal is concentrated between 8 and 28 msec, and therefore, only this portion is used for all further analysis.

The cosine distance between $|\Theta_{\text{pre}}|$ and $|\Theta_{\text{post}}|$ was calculated for all the rats and limbs. The mean difference between the cosine distances of forelimbs (non-injured) and hindlimbs (injured) was checked for significance using a student's paired sample two-tailed t-test. These cosine distance values were also used to compute the different performance measures. The best cut-off point was calculated from the ROC curve as the closest point to the $(0, 1)$ coordinate point. These results were published recently in Ref. [25].

3.3.2. The Phase Space Analysis of SEP

In an effort to characterize the entire morphology of a particular SEP sweep, we have further developed another analysis for quantification, which uses the modern concepts

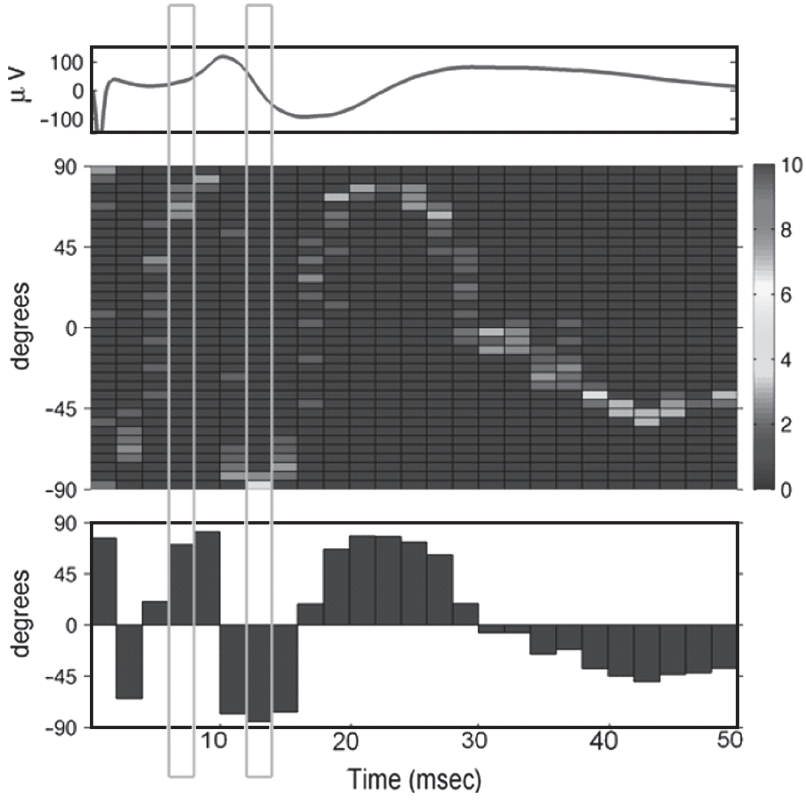

Figure 11. A sample SEP signal (middle), its slope histogram (top), and its mean slope vector Θ (bottom). A single rectangle (in magenta) corresponds to a single time bin of 2 msec. consisting of 10 samples. In the slope histogram, the angular orientations $\theta[k]$ in a single time bin are color coded in angle bins of 5 degrees.

borrowed from nonlinear time series analysis tools. This is the so-called "Phase Space Analysis" of the SEP.

Thus, we propose studying SSEPs using a dynamical systems perspective in the phase space or state space. In order to obtain the phase space curve for a SSEP waveform we plot its first time derivative against its magnitude. In doing this, we parameterize the magnitude and its rate of change as a function of time, thereby capturing not only the amplitude information but also potentially useful information about the signal morphology. Since phase space of the signal takes the entire waveform into consideration, under the assumptions of similar recording conditions, this method has the potential to replace traditional methods of SSEP analysis, with higher sensitivity and specificity, without requiring the averaging of as many sweeps and manual intervention. Thus, we propose to use the phase space representation of the SSEP to create a simple automated graphical and quantitative tool to characterize SSEP waveforms.

The phase space is the set of all possible states of a system with each state occupying a distinct point. In the context of second-order dynamical systems, phase space consists of the position and the momentum (or velocity) variables, as these two pieces of information completely determine the temporal evolution of the dynamical system. Phase-space analysis is also often used in biological settings when a two-parameter model of a complex biological process is created. In the context of SSEPs, we focus on the signal amplitude and the rate of change of the signal amplitude, or its first derivative. While the signal amplitude at any given point is indicative of the level of stimulation of the neural tissue at the point, the rate of change of amplitude is indicative of the conduction velocity of the neural tracts involved. In order to use the information contained in the shape of the waveform, we study the entire signal along with its rate of change at every time point.

Consider a time-varying signal $x(t)$; its representation in the phase-space domain is the set of points $(x(t), dx(t)/dt)$ where $dx(t)/dt$ is the first derivative of $x(t)$. In the case of a digitized version $x[n]$ of a continuous signal $x(t)$ sampled at a frequency f_s the derivative $x'(t)$ can be approximated by using Newton's Difference Quotient as follows:

$$x'(t) \approx \frac{\Delta x[n]}{\Delta n} = \frac{x[n + t_s] - x[n]}{t_s}; \quad t_s = 1/f_s \tag{12}$$

This method of computing derivatives is also known as "finite differencing." While the real slope of the signal at any point can be geometrically represented by the slope of the tangent to that point, this equation uses the slope of the secant line between two consecutive closely spaced points to approximate slope.

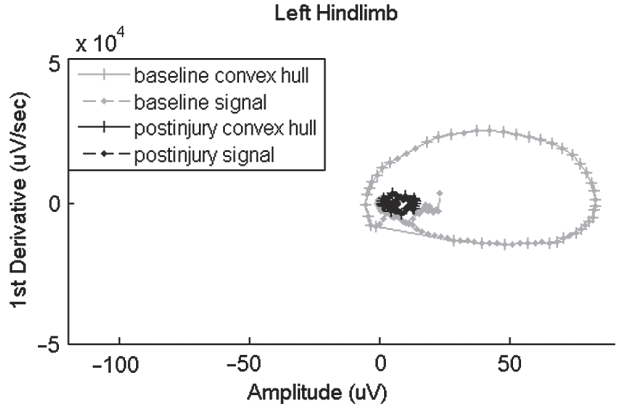

Figure 12. This figure shows an SEP signal in the phase plane. The signal is plotted in a red dashed line, with each sampled point being denoted by a "+." The convex hull of the signal is plotted in a continuous line, in blue.

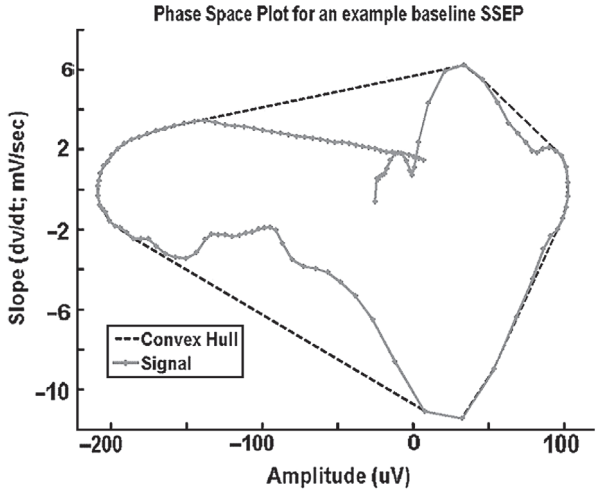

Figure 13. A typical phase space plot for SEP before and after a spinal cord injury in a rat. Baseline SEPs are plotted in red and post-injury SEPs in blue. Note the marked reduction in Phase Space Area (PSA).

Plotting the signal and its derivative yields the representation of the signal in the phase domain. We define this transformed waveform as the phase space curve (PSC). While the signal itself dictates the shape of the PSC, the area bounded by the curve is indicative of the *power content* in the signal, which is of importance in the study of neurological injury models that may affect conduction in the somatosensory pathway.

In order to compute the area bounded by the PSC, we first fit a convex hull to it. In computational geometry, a convex hull of a set of points P in a real vector space is the minimum convex set spanning P. Analogous to the manner in which a stretched rubber band takes the shape of the object it is placed around, the convex hull, a simple closed polygon chain, captures the "extent" of a non-empty set of points in a planar sense. Several algorithms have been developed to compute the convex hull, and we used the Quickhull algorithm described by Barber et al. [26]. In order to quantify the transformed waveform, we compute the area enclosed by the curve, termed the phase space area (PSA), using numerical integration as shown in Figure 12.

Typical phase space plots before and after severe spinal cord injury are shown in Figure 13 for our rat model of contusive spinal cord injury. The depicted curves are for SEP upon the left hindlimb stimulation.

We have obtained the best sensitivity and specificity for the phase space area technique using different metrics for normalizations—either with respect to pre-injury data or in the context of our thoracic spinal cord injury model, with respect to the forelimb SEP, which do not change significantly after injury at the thoracic level.

Table 2 below shows the sensitivity and specificity for the phase space area method using these different normalization techniques.

Table 2. The sensitivity and specificity for the phase space area method using different normalization techniques.

Type of analysis	Method	Measure	Contusion injury (%)
Phase space analysis	Percentage change in PSA relative to baseline	Specificity	87.50
		Sensitivity	75.00
		Threshold	32.00
	Forelimb normalized change in PSA	Specificity	100.50
		Sensitivity	91.67
		Threshold	45.00
	Hindlimb-Forelimb PSA Ratio	Specificity	79.17
		Sensitivity	91.67
		Threshold	11.00

The phase space area method, developed mainly to characterize the entire morphology of the SEP response curve, utilizes modern concepts from nonlinear time series analysis and could be potentially useful in the future for developing a simple, graphical as well as quantitative tool for real-time monitoring of nervous system injuries, for example, in spinal cord injury patients or in intra-operative monitoring during brain surgeries.

4. DISCUSSION AND CONCLUSIONS

In all acute cord syndromes, the full extent of injury may not be apparent initially. Hence, long-term as well as immediate assessment of injury and recovery is warranted. Most of the time a routine clinical examination, especially in the acute phase, will not detect the presence of uninjured fibers. This is a misdiagnosis for patients with SCI. Even a small number of uninjured fibers after spinal cord injury with correct treatment can make a huge difference in the quality of life of patients and in society. If some sensory-motor function is persevered, the chance that the patient will eventually be able to walk is greater than 50%. Ultimately, 90% of patients with SCI return to their homes and regain independence. In the early 1900s, the mortality rate one year after injury was 100%. Currently, the five-year survival rate for patients with a traumatic quadriplegia exceeds 90%, and we strongly believe survival and quality of the lives of these patients could be even higher if physicians have full knowledge about the primary injury in the acute phase. Knowledge about the uninjured fibers sooner rather than later will help physicians to plan strategic treatment and limit primary injury and devise ways to prevent progression of the injury into the secondary phase. Hence, the long-term goal of this research has been to develop alternative technologies for monitoring the spinal cord, measuring the injury, and assessing the benefit of therapeutic treatments to the spinal cord for basic scientists as well as clinicians. We have focused on the bio-engineering aspect of this medical issue to provide novel technology and quantitative methods to determine the injury extent and recovery of the axonal pathways in a two-pronged approach to study the function and structure through complementary technologies.

We have determined the electrophysiological response of the spinal cord sensory pathways. The core bioengineering concept was studying functional recovery by electrophysiological monitoring and quantitatively analyzing multi-channel somatosensory evoked potentials by determining the electrophysiological sequence of the injury and its evolution from primary and secondary injuries with the help of advanced signal processing techniques. The techniques presented in this chapter included spectral coherence, correlation-based metric, entropy-based metric and morphological analysis.

Our presented work will decisively aid clinicians in their quest to rigorously determine the success of their therapeutic strategies. The recent interest and advances in spinal cord injury therapies ranging from cell based, gene therapy, and tissue engineering would benefit by having the tools to objectively identify injury and the subsequent delivery of therapeutics to aid recovery of spinal tract function. We expect these methods to aid clinicians in non-invasively assessing the progression of spinal cord injury physiological response.

REFERENCES

1. E. N. Marieb, "Essentials of Human Anatomy & Physiology," 9th edition. Pearson Education, 2009.
2. Divisions of Spinal Segments, http://en.wikipedia.org/wiki/File:Gray_111_-_Vertebral_column-coloured.png.
3. E. Niedermeyer, "Electroencephalography, Basic Principles, Clinical Applications, and Related Fields," 4th edition. Lippincott, Williams and Wilkins, Philadelphia, Pennsylvania, 1999.
4. Spinal Cord Injury Facts, Updated June, http://www.fscip.org/facts.htm (2009).
5. J. Qiu, *Lancet Neurol.* 8, 606 (2009).
6. W. A. Truccolo, M. Ding, K. H. Knuth, R. Nakamura, and S. L. Bressler, *Clin. Neurophysiol*. 113, 206 (2002).
7. N. B. Finnerup, C. Gyldensted, A. F. Frederiksen, F. W. Bach, and T. S. Jensen, *Acta Neurol. Scand.* 109, 194 (2004).
8. M. Nuwer, *Muscle Nerve* 22, 1620 (1999).
9. M. Shepard and M. Bracken, *Spinal Cord* 37, 833 (1999).

10. O. A. Glenn and J. Barkovich, *Amer. J. Neuroradiol.* 27, 1807 (2006).
11. D. Basso, M. Beattie, and J. Bresnahan, *J. Neurotrauma* 12, 1, (1995).
12. D. Basso, M. Beattie, and J. Bresnahan, *Exp. Neurol.* 139, 244 (1996).
13. N. Fatoo, N. Mirza, R. Ahmed, H. Al-Nashash, N. Thakor, and A. All, "Detection and Assessment of Spinal Cord Injury Using Spectral Coherence," Proc. IEEE Conf. Eng. Med. Biol. Soc., 2007, pp. 1426–1429.
14. A. All, N. Fatoo, N. Mirza, R. Ahmed, H. Al-Nashash, and N. Thakor, "Using Spectral Coherence for the Detection and Monitoring of Spinal Cord Injury," presented at the GCC Ind. Electr. Electron. Conf., Manama, Bahrain, 2007.
15. G. Agrawal, C. Kerr, N. V. Thakor, and A. H. All, "Characterization of Graded MASCIS Contusion Spinal Cord Injury using Somatosensory Evoked Potentials," *Spine Journal*, accepted Aug. (2009).
16. M. Rangaraj, "Biomedical Signal Analysis: A Case Study Approach." Wiley/IEEE Press, New York/ Piscataway, NJ, 2002.
17. S. Stearns and R. David, "Signal Processing Algorithms." Prentice-Hall, Englewood Cliffs, New Jersey, 1988.
18. H. Al-Nashash, N. Fatoo, N. Mirza, R. Ahmed, G. Agrawala, N. Thakor, and A. All, *IEEE Transactions on Biomedical Engineering* 56, 1971 (2009).
19. H. Mir et al., "Quantification of Spinal Cord Injury Using Somatosensory Evoked Potentials," 2010 International Conference on Bioinformatics and Biomedical Engineering, June, 2010.
20. H. Mir et al., "Histogram Based Quantification of Spinal Cord Injury Level Using Somatosensory Evoked Potentials," IEEE Conference on Engineering in Medicine and Biology, September, 2010.
21. J. Lian et al., *Signal Processing* 684 (2009).
22. T. Cover and J. Thomas, "Elements of Information Theory." Wiley, 1991.
23. C. Maciel, J. Pereira, and D. Stewart, *IEEE Sig. Proc. Mag.* 27, 120123 (2010).
24. L. Lee, "Measures of Distributional Similarity," Proc 37th Ann Meet Assoc Comput Linguist, pp. 25–32, 1999.
25. G. Agrawal, D. Sherman, A. Maybhate, M. Gorelik, D. Kerr, N. Thakor, and A. Al, *J. Clin Neurosci.* 17, 1159 (2010).
26. C. Barber, D. Dobkin, and H. Huhdanpaa, *ACM Transactions on Mathematical Software (TOMS)* 22, 469 (1996).